

The Gamma-ray burst 050904 : a star in the early sky

B. Gendre¹, A. Galli^{1,2,3}, A. Corsi^{1,2,4}, A. Klotz^{5,6}, L. Piro¹, G. Stratta⁷, M. Boër⁶, and Y. Damerjji^{6,5}

¹ IASF-Roma/INAF, via fosso del cavaliere 100, 00133 Roma, Italy

e-mail: bruce.gendre@iasf-roma.inaf.it, alessandra.corsi@iasf-roma.inaf.it, galli@iasf-roma.inaf.it, piro@iasf-roma.inaf.it

² Università degli Studi di Roma "La Sapienza", Piazzale A. Moro 5, 00185, Roma, Italy

³ INFN - Sezione di Trieste c/o Dipartimento di Fisica – Università di Trieste Via Valerio 2, 34127 Trieste, Italy

⁴ INFN - Sezione di Roma c/o Dipartimento di Fisica – Università degli Studi di Roma "La Sapienza" Piazzale A. Moro 5, 00185 Roma, Italy

⁵ CESR, 9 avenue du Colonel Roche, 31400 Toulouse, France

e-mail: klotz@cesr.fr

⁶ Observatoire de Haute-Provence, 04870 St Michel l'Observatoire, France

e-mail: michel.boer@oamp.fr

⁷ LATT, Observatoire Midi-Pyrénées, 14 avenue Edouard Belin, 31400 Toulouse, France

e-mail: gstratta@ast.obs-mip.fr

Received —; accepted —

ABSTRACT

Aims. We present optical and X-ray observations of GRB 050904 obtained with TAROT and SWIFT.

Methods. We perform temporal and spectral analysis of the XRT and optical data.

Results. We find evidence for a variable absorption in the early phase of the afterglow and we interpret this as a progressive photo-ionization. The spectral properties of the early X-ray flare observed about 460 seconds after the burst are similar to those of the following afterglow. In the optical band, we observe a flare simultaneous with the X-ray one. We use the temporal and spectral information to interpret the data. The overall behavior of the early afterglow is compatible with a fireball expanding in a wind environment, and the late optical flattening might be explained by the effect of a termination shock. To explain the simultaneous X-ray and optical flares we consider the hypothesis of delayed external shock from a thick shell, inverse Compton emission from reverse shock, reverse shock from synchrotron emission, inverse Compton emission from late internal shock or a very long internal shock activity.

Key words. Gamma-ray : burst – X-ray : general – Star : general

1. Introduction

Long Gamma-Ray Bursts (GRBs) are thought to be produced by a massive star (MacFadyen & Woosley 1999). Their extreme luminosity (up to $L_{iso} \sim 10^{53}$ erg s⁻¹, Piran 2005) makes them observable up to very large distance ($z > 5$). Their long lasting afterglow allows one to study them for days after the trigger (for a review see Zhang & Meszaros 2004; Piran 2005). At large distance, the time dilation due to cosmological effects makes more easy any study on the early afterglow phenomenon.

With the launch of the SWIFT satellite (Gehrels et al. 2005), it has been shown that strong flaring activity in the early X-ray afterglow is a common phenomenon (O'Brien et al. 2006). The origin of these X-ray flares is not clear, and several models have been proposed: late internal shock (Fan & Wei 2005; Burrows et al. 2005b), refreshed energy injection due to

long lasting activity of the GRB progenitor (Zhang et al. 2005), rising of an extra spectral component such as inverse Compton (Kobayashi et al. 2005), late internal and external shocks (Wu et al. 2006), delayed external shock emission in a thick shell fireball (Piro et al. 2005; Galli & Piro 2005). While some of these flares show spectral evolution and may be linked to the prompt emission (Burrows et al. 2005b), others look very similar to the late afterglow emission and can be linked to its onset (Piro et al. 2005; Galli & Piro 2005). Nevertheless, no multi-wavelength observations are usually available to discriminate these hypothesis, and several models can fit the data (e.g GRB 050406, Wu et al. 2006).

Another interesting aspect of the early afterglow evolution is the problem of the surrounding medium of the burst. As long GRBs are due to massive stars, one should expect around them a wind environment (Chevalier et al. 2004). On the other hand, it has been observed around several GRBs a constant density medium (hereafter InterStellar Medium, or ISM) not compat-

ible with a wind environment (Panaitescu & Kumar 2001). Several authors (e.g. Ramirez-Ruiz et al. 2001) proposed that the expanding wind arising from the star can be blocked by a dense surrounding interstellar medium. The interface between these two media is called the termination shock. This termination shock was never directly observed so far, while its presence should be observed in the afterglow spectra and light curve (Chevalier et al. 2004; Ramirez-Ruiz et al. 2001).

In previous articles (e.g. Watson et al. 2006; Boër et al. 2006; Tagliaferri et al. 2005b), several specific wavelength analysis of GRB 050904 have been published. In this article, we will expose a multi-wavelength analysis of this burst. It presented strong and long lasting multi-wavelength flaring activities and occurred at $z = 6.29$ (Kawai et al. 2005; Watson et al. 2006; Boër et al. 2006). This allows a detailed study of the early part of the afterglow, and in particular the analysis of any short time scale events. We summarize previous observations in Sec. 2 and describe the data analysis in Sec. 3. We report in particular a more detailed analysis of the X-ray and TAROT data. We investigate the surrounding medium properties and the possible progenitor nature in Sec. 4. We discuss the origin of the observed multi wavelength flare in the framework of a delayed external shock emission due to a thick shell fireball in Sec. 5.1. Other models proposed in the literature are discussed in Sec. 5.2. Conclusions are given in Sec. 6.

2. GRB 050904

GRB 050904 was triggered by the BAT instrument (Barthelmy et al. 2005) on board the SWIFT satellite (Gehrels et al. 2005) on September 4th, 2005, at 01:51:44 UT (Cummings et al. 2005). This was a bright burst, with a fluence of $5.4 \pm 0.2 \times 10^{-6}$ erg cm $^{-2}$ (15–150 keV), and a duration of $T_{90} = 225 \pm 10$ seconds (Sakamoto et al. 2005). The energy spectral index was 0.34 ± 0.06 (Sakamoto et al. 2005). The narrow field instruments XRT (Burrows et al. 2005) and UVOT (Mason et al. 2005) observed the field of GRB 050904 about 160 seconds after the trigger. No optical counterpart was observed within the UVOT field of view, while an X-ray transient was detected at position $00^h 54^m 50.4^s +14^\circ 05' 08.5''$ (Cummings et al. 2005). The first optical detection was made by TAROT (Boër et al. 1999), which observed a faint optical afterglow in a clear filter (Klotz et al. 2005b,c; Boër et al. 2006). Other observations made with the BOOTES-1B telescope failed to detect this afterglow in the R band (Jelinek et al. 2005). Larger optical and infrared telescopes imaged the field of view 3 hours after the burst and detected an infrared counterpart (Haislip et al. 2005). The absence of any counterpart observed from the R to U bands implied a large absorption, possibly due to the Lyman alpha forest (Haislip et al. 2005). This was confirmed by the spectroscopic redshift measured by the Subaru telescope ($z = 6.29$ Kawai et al. 2005), which implied that the Lyman alpha cut-off was redshifted in the optical up to the I band. This burst is currently the more distant burst ever observed.

3. Data reduction and analysis

3.1. X-ray data

3.1.1. Data reduction

We obtained the XRT data from the SWIFT archive¹ and reduced them using the available packages and calibration files (SWIFT FTOOLS version 2.2 and CALDB version 20051028). Data were filtered using the provided good time intervals (sun and moon constraints, bright earth and South Atlantic Anomaly limitations) and standard criteria : CCD temperature $< -50^\circ\text{C}$; grades 0 to 2 and energy above 0.3 keV for Window Timing mode (WT); grades 0 to 12 and energy above 0.5 keV for Photon Counting mode (PC). Note that the spectral ranges are different in WT and PC mode to take into account some uncertainties of the PC mode calibration (Osborne et al. 2005). We extracted spectra and light curves using circle (PC mode) or box (WT mode) regions of 25 pixels radius (that enclose $\sim 95\%$ of the PSF). The background was estimated using a larger region free of sources.

Our filtering criteria are mode dependent due to the spectral range change, and the change of mode may introduce some problems due to cross calibration uncertainties. Thus, any count light curve extracted need to be corrected for this dependency. To do so, we constructed a color-color diagram to look for spectral variability. This information allowed us to convert the count light curve into a flux one which is mode independent. This light curve is presented in Fig. 1. As one can see, the transition between the two modes occurs at the end of a large flare; however, the continuity of the light curve made us confident on our analysis.

We extracted spectra for several time intervals listed in Table 1. The spectra were re-binned to contain at least 20 net counts per bin using GRPPHA, and were fitted using XSPEC version 11.3.1 (Arnaud 1996).

3.1.2. Data analysis

The X-ray light curve shows a steep decrease of the early part of the data, followed by a plateau and a large flare (see Fig. 1). Other flares occurs later in the light curve. We fitted the first part of the light curve (< 2000 s), excluding all the X-ray flares, using a simple power law. We obtained a decay index of $\delta = 2.44 \pm 0.08$ ($\chi^2_\nu = 1.12$, 29 d.o.f.). However, this power law is not consistent with the late (> 2000 s) data (see Fig. 2). Moreover, an analysis of the residuals showed systematic deviations indicating a poor fit. As we observed a sudden softening of the spectrum after $t = 384$ s, we tried to fit the data using a broken power law. This model can also describe the data, with an early decay of 2.45 ± 0.2 and a late decay of 1.5 ± 0.2 ($\chi^2_\nu = 0.99$, 26 d.o.f.). The two power law segments connect at the end of the first flare.

The whole spectra (0.3 or 0.5 to 10 keV) were fitted with a simple power law (i.e. $F(\nu) \propto \nu^{-\alpha}$), absorbed by our galaxy (N_H value fixed to the galactic one of 4.97×10^{20} cm $^{-2}$ Dickey & Lockman 1990) and by the host galaxy at redshift 6.3. We

¹ see <http://swift.gsfc.nasa.gov/docs/swift/archive/>

detect an excess of absorption only in the early WT data (before 464 s). After that, we have only upper limits. Because of the large redshift, we cannot set a meaningful constrain on the host column density with the PC mode restricted to energies above 0.5 keV, as already noted by Watson et al. (2006). Thus, in order to better constrain the spectral index, we fixed the extragalactic column density value to zero for the PC mode (after 596 seconds). Results from this spectral analysis are listed in Table 1. These results are in agreement with those published by Watson et al. (2006). We note however that these authors reported an increase of the N_H in the late afterglow. An inspection of the residuals indicated a very poor fit between 2000 and 10000 seconds ($\chi^2_\nu = 2.04$, 42 d.o.f.). As stated above, adding some absorption locally to the burst fail to improve significantly the fit ($\chi^2_\nu = 2.03$, 41 d.o.f.), and resulted only in an upper limit (however, this upper limit is consistent with the value reported by Watson et al. 2006). This poor fit could be due to some spectral component of the flares occurring between 2000 and 10000 seconds, we do not investigate it further.

We restricted the analysis to the early data (<2000 s). Figure 3 shows the variations of the softness ratio, the spectral index and the extragalactic column density as a function of time. The softness ratio is computed by dividing the counts detected in the 0.5-2.0 keV band by those detected in the 2.0-10.0 keV band (i.e. the soft band is affected by absorption, while the hard band is not affected). We observe a global softening of the spectrum with time. Before the flare, the softening, very progressive, is correlated with a decrease of the N_H value. We can confidently exclude a constant N_H value hypothesis ($\chi^2/dof = 14/4$), while an exponential decay as $N_H(t) = N_H(0)e^{(-t/\tau)}$ fit the data ($\chi^2/dof = 4/4$, see Fig. 3). Expressed in the rest frame, the best fit parameters are $N_H(\tau) = 3.7 \pm 2 \times 10^{24} \text{ cm}^{-2}$ and $\tau = 6.2\text{s}$. At the start of the flare, the softness ratio changes suddenly to a softer value. At the maximum of the flare, we note a brief and transient change of the softness ratio, that becomes harder. Simultaneously, the measured N_H features a peak. We note a last transient change of the softness ratio at $t = 600\text{s}$ (all these changes will be discussed in Sec. 4, 5.1 and 5.2). After that, it remains constant (even during the second flare). Figure 3 also shows the variations of the energy spectral index. This spectral index is constant before the first flare, changes of value at the start of this flare, and remains constant during and after the flare. A spectral fit on all the WT data before and after the start of the flare indicate a power law energy index of 0.23 ± 0.05 and 0.57 ± 0.06 respectively ($\chi^2_\nu = 1.2$, 288 d.o.f.). This latter value is consistent with the one derived from the following PC data (0.53 ± 0.09).

3.2. Optical data

TAROT (*Télescope à Action Rapide pour les Objets Transitoires*) is a robotic observatory designed for GRB early detections (e.g. Klotz et al. 2005a). The telescope diameter is 25 cm, the camera is equipped by a CCD Marconi 42-40 (2048x2048 pixels of $13.5\mu\text{m}$) thin back illuminated. The spatial sampling is 3.3 arcsec/pixel.

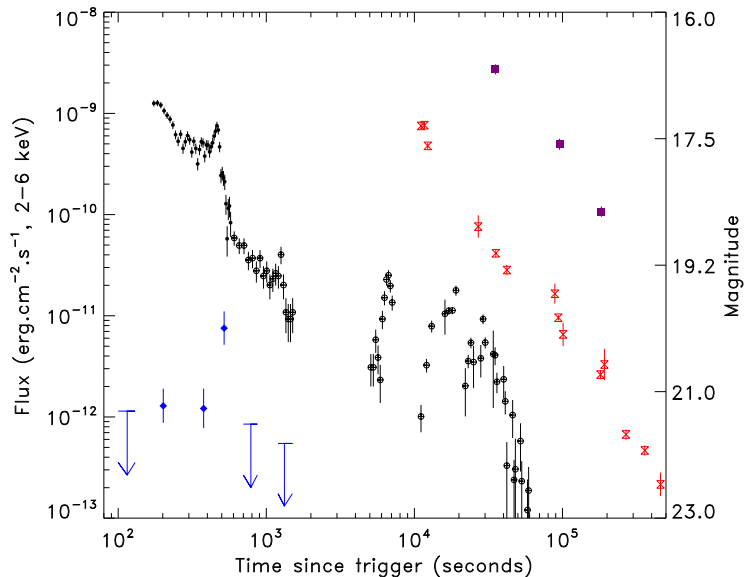


Fig. 1. Multi-wavelength light curve of GRB 050904. We present the X-ray data taken in the 2.0-6.0 keV band with filled black circles (WT mode data) and open black circles (PC mode data), the TAROT I_T band data with blue diamonds, the H data with solid purple squares (from Haislip et al. 2005; Tagliaferri et al. 2005b) and the J data with open red symbols (from Haislip et al. 2005; Tagliaferri et al. 2005b). For clarity, offsets by +6 and -1.5 magnitudes have been applied to TAROT data and H band data respectively. See electronic version for colors.

Table 1. X-ray (0.3 or 0.5 keV to 10.0 keV band) spectral fitting results. The χ^2_ν value of the fit is 1.26 for 463 degrees of freedom. The Extragalactic absorption is given at $z = 6.3$.

Temporal slide (s)	Extragalactic absorption (10^{22} cm^{-2})	Energy index α
169-202	18 ± 5	0.2 ± 0.2
203-264	$4.7^{+3.3}_{-2.8}$	0.2 ± 0.1
264-384	< 1.93	0.24 ± 0.06
384-463	$5.3^{+3.0}_{-2.6}$	0.65 ± 0.1
464-581	< 1.50	0.54 ± 0.06
596-979	—	0.53 ± 0.09
986-1666	—	0.7 ± 0.2
2000-10000	—	0.73 ± 0.08
10000-20000	—	0.74 ± 0.07
20000-	—	0.82 ± 0.08

The Gamma-ray burst Coordinate Network (GCN) distributed the SWIFT alert 81 s after the beginning of the prompt emission of GRB 050904. The TAROT first exposure begun five seconds later. Twenty two unfiltered CCD images were taken between UTC 01:53:10.2 ($t_{\text{trig}}+86.2\text{s}$) and 02:08:09.6 ($t_{\text{trig}}+1666.4\text{s}$). Two technical problems occurred during the record:

- i) A bug of the scheduling software lead to stop observations in the range $t_{\text{trig}} + 254$ to $+312\text{s}$.
- ii) The CCD camera cooler stopped due to a wire that broke during the fast slew of the telescope. As a consequence, the

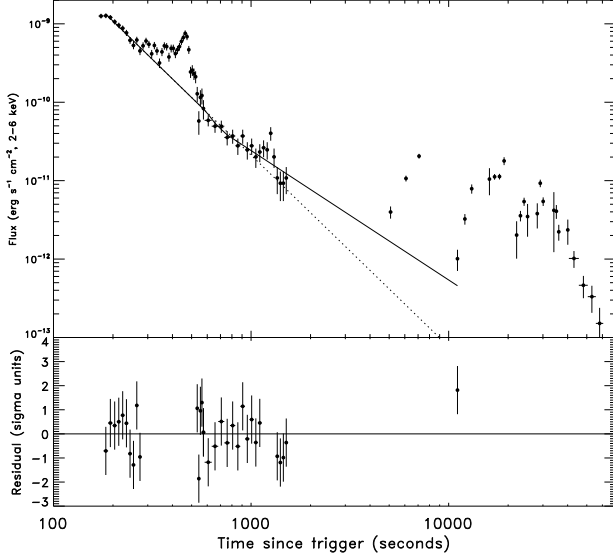


Fig. 2. Top panel : the X-ray light curve of GRB 050904 fitted with a simple power law (dashed line) and a broken power law (solid line), excluding the bright flares. Bottom panel : residuals of the broken power law fit.

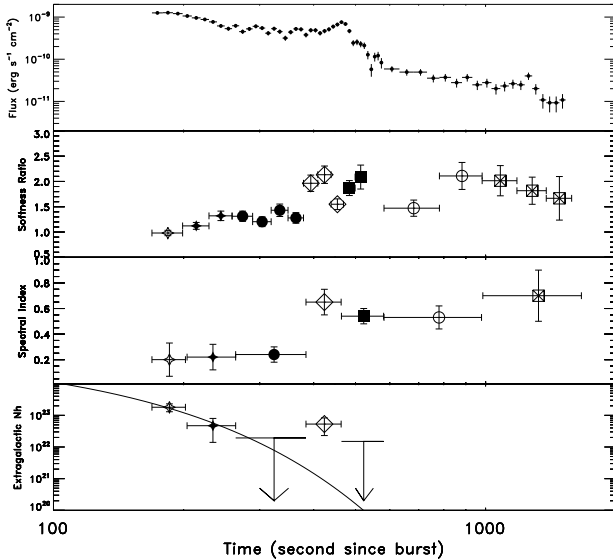


Fig. 3. First panel (Top) : X-ray light curve of the early afterglow of GRB 050904 in the 2.0-6.0 keV band. We have converted the count rate in flux using the conversion factors derived from our spectral analysis. Second panel) : The softness ratio of the X-ray afterglow (0.5-2.0 keV band versus the 2.0-10.0 keV band). Third panel) : The energy index of the afterglow spectra. We assumed for each spectra the same absorbed power law model. Last panel (Bottom) : the extragalactic column density obtained from the fit to the data, together with the best fitted decay law (see text). Note that the current calibration of the PC mode does not allow us to fit this quantity in the PC spectra. The symbols in panels b), c), and d) refer to the temporal slides listed in Table 1.

temperature of the CCD remained at -50°C until $t_{trig}+260\text{s}$ and then increased continuously to $+14^{\circ}\text{C}$ at $t_{trig}+1500\text{s}$. Frames taken after $t_{trig}+590\text{s}$ are strongly affected by thermal noise.

We co-added frames into 6 final images in order to increase the signal to noise ratio.

Table 2. Reference star characteristics nearby the position of GRB 050904.

2MASS	I	V-R	V-I	Sp. Type
013.693725	11.68	0.70	1.31	K4V
013.732724	12.29	0.49	1.01	K2V
013.782866	12.39	0.35	0.74	G0V

Calibrations of TAROT data are difficult because images were acquired with no filter, and the high z of the GRB induces a non standard spectrum over the optical wavelengths. First, we choose three stars separated by less than 5 arcmins from the GRB and we calibrated their VRI magnitudes with the 80 cm telescope at the *Observatoire de Haute-Provence*, using stars of the SA92 field of calibration (LONEOS 2003). We completed this study with spectra taken with the same telescope equipped by a low resolution spectrograph ($R=150$), and fit the star continua. Results of photometry, spectrometry and data from 2MASS catalog allowed us to attribute accurate magnitudes and spectral types (see Table 2). We computed the so called *superstar* as the sum of the three reference stars using the stellar spectral flux library provided by Pickles (1998). For each TAROT image, we computed the Point Spread Function (PSF) of the *superstar*. We fit the optical transient (OT) of GRB 050904 by this PSF searching the a coefficient corresponding to the minimum value of the $(OT - a \times \text{PSF})^2$. To calibrate the flux of the OT, we assumed a spectral index $\beta=-1.2$ and a sharp cut-off at $\lambda=8862 \text{ \AA}$. We modeled the response of the system (atmosphere, optics and CCD) and we applied it to the theoretical spectra of the OT and to the *superstar*. Then, we adjusted the flux of the OT at $\lambda=9500 \text{ \AA}$ to obtain the same a coefficient than that obtained from TAROT images (we call this “filter” the I_T band). Results are reported in Table 3, and presented together with the X-ray data in Fig. 1. As one can see, and as already reported in Boër et al. (2006), TAROT has observed a flare in the I_T band which is coincident with one X-ray flare.

Table 3. Flux derived from TAROT images. In parenthesis, upper limit computed from PSF fit using a signal-to-noise (S/N) limit 3.

t_{trig} range (s)	Flux at 9500 \AA ($\text{ergs cm}^{-2} \text{ s}^{-1} \text{ \AA}^{-1}$)	S/N
86 - 144	$(7.5 \times 10^{-16}) < 5.3 \times 10^{-15}$	<2
150 - 253	$4.6 - 7.4 \times 10^{-15}$	3.7
312 - 443	$4.2 - 7.4 \times 10^{-15}$	3.1
449 - 589	$1.3 - 2.1 \times 10^{-14}$	4.0
595 - 978	$(4.2 \times 10^{-15}) < 4.2 \times 10^{-15}$	2.7
985 - 1666	$(2.5 \times 10^{-15}) < 3.1 \times 10^{-15}$	<2

We completed these optical observations with observations reported in Tagliaferri et al. (2005b) and Haislip et al. (2005) (see Fig. 1). It has been reported in optical a steep-flat-steep evolution (Haislip et al. 2005; Tagliaferri et al. 2005b). From an initial decay of 1.36 ± 0.07 between 0.125 and 0.5 days (Haislip et al. 2005), the light curve flattens to a decay of 0.7 ± 0.2 . At 2.6 ± 1.0 days, the light curve steepens to a decay of 2.4 ± 0.4 , as usually observed in case of a so-called jet break (Rhoads 1997).

4. The global afterglow analysis

4.1. The spectral evolution of the X-ray afterglow

The hard γ -ray emission is observed up to the start of the first X-ray flare ($t \sim 420$ s) (Sakamoto et al. 2005). Moreover, the X-ray emission before the first flare ($t = 169\text{--}400$ s) has temporal ($\delta = 2.45 \pm 0.2$) and spectral ($\alpha = 0.2 \pm 0.1$) indexes compatible with the tail of the prompt one, i.e. with off-axis emission (closure relationship $\delta = 2 + \alpha$, Kuman & Panaitescu 2000), and the X-ray spectral index observed before the start of the flare is comparable to the gamma-ray one (0.2 ± 0.1 vs 0.34 ± 0.06 respectively). Thus, the XRT observation starts during the prompt phase of the burst. During this phase (thus before the beginning of the first flare), we observe a significant softening of the X-ray spectrum. This softening has been observed in several other GRB afterglows (e.g. GRB 011121, GRB 050219A, Piro et al. 2005; Tagliaferri et al. 2005a). GRBs harbor a well known hard-to-soft evolution of the prompt emission, and this softening can be due to the prompt standard spectral evolution. Another more interesting possibility would be that the softening is due to the observed decrease of the column density. Such a decrease has been already observed in previous bursts, such as GRB 000528 (Frontera et al. 2004) and GRB 980329 (Frontera et al. 2000; Lazzati & Perna 2002) although, in these cases, the available statistics were too low to exclude a constant N_H . The exponential decrease of the measured equivalent column density that we observe in the case of GRB 050904 may be the evidence of a progressive photoionization of the initially cold gas in which the GRB occurs by the burst itself (Lazzati & Perna 2002). Another explanation could be that the blast wave has crossed a medium with a larger density, such as a clump of matter.

A significant softening is observed at the start of the first flare; the softness ratio remains constant through the flare except at the maximum of the flare (~ 460 s, see below). This variation is accounted for by the model with an increase of the column density (see Table 1, bin 4). This is really surprising as one should not expect such an increase. A final analysis of the data at the peak shows that this hardening is concentrated in a very short interval (10s) Excluding this small time interval from the data and extracting again a spectrum, we do not observe anymore this increase of N_H . A possible explanation could be the emergence of an inverse Compton emission (see Sec. 5.2). We note however that except this deviation, both the column density and the spectral index are constant; moreover the spectral index measured is consistent with the one observed between 1 and 2 ks.

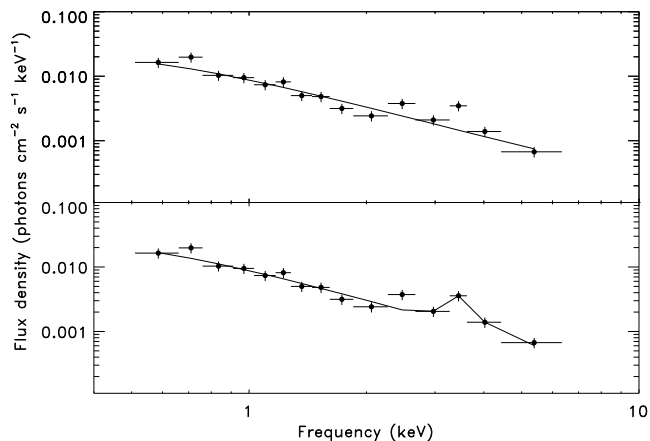


Fig. 4. The X-ray spectrum of GRB 050904 integrated between 582 and 978 seconds after the burst. Top : fitted with a single power law. Bottom : fitted with a power law continuum and a Gaussian line at energy 3.46 keV.

At $t=582$ s, another hardening is observed. Very surprisingly, the spectral index does not vary and no excess of absorption is detected at that time (see Sec. 3.1.2). However, the spectral fit of this part of the data is very poor ($\chi^2_\nu = 2.1$, 13 d.o.f.). A fit with a two component model (e.g. a hard power law plus a soft power law, as expected if we observe the afterglow together with a significant signal from the tail of the prompt emission) is even worse ($\chi^2_\nu = 2.4$, 11 d.o.f.). As can be seen from Fig. 4, the main discrepancy arises from a bin at about 3.3 keV. We have tried to fit it with a narrow line. We obtain a better agreement with a line at 3.46 ± 0.15 keV with $\sigma < 0.46$ keV ($\chi^2_\nu = 1.34$, 10 d.o.f.). The continuum parameter changes to $\alpha = 0.66 \pm 0.17$. Using this continuum model, we match a softness ratio of 1.9, compatible with the hypothesis that the softness ratio is constant after the first flare. This change of the softness ratio may thus be due only to that discrepancy at high energy. However, this deviation is due to only one bin, and the statistic does not allow us to discriminate between a spurious deviation and a real emission line. In the latter case, this turns to be a line emitted at the energy of 25 ± 1 keV in the rest frame.

After the initial 2 ks of data, the XRT light curve features several flares (see Fig. 1). X-ray spectra extracted during the 3rd, 4th and 5th flares indicate a small softening of the spectral properties. We cannot investigate the underlying decay law due to the large flaring activity.

4.2. The progenitor and surrounding medium of GRB 050904

The observed spectral index after the first flare is very low (0.57 ± 0.06), compared to the common value of ~ 1.1 observed in BeppoSAX, XMM-Newton or Chandra afterglows (Gendre et al. 2006; De Pasquale et al. 2006). On the other hand, the temporal decay has a more common value (1.5 ± 0.2). This combination of low spectral index and normal temporal decay was observed only in the case of GRB 040106, which was claimed

by Gendre et al. (2005) to be surrounded by a stellar wind. We thus have checked using the closure relationships given by Sari et al. (1998), Chevalier & Li (1999), and Sari et al. (1999) if a wind medium was possible in the case of GRB 050904. The results are listed in Table 4. As one can see in that table, jet effects are discarded during the early afterglow. The constant density medium does not fit the observed data, while a wind medium can fit the data, if the cooling frequency is above the X-ray band. Assuming that this wind arises from the progenitor of GRB 050904, we thus can indicate that this progenitor is a massive star.

The optical data can also give insight into the surrounding medium of GRB 050904. We will separate them for clarity between *early* and *late* optical data as observed before and after 0.5 days. This date is chosen because both Haislip et al. (2005) and Tagliaferri et al. (2005b) observe a flattening at that time. The *early* optical data agree with the X-ray findings; in particular its decay index is consistent with the X-ray one. The *early* optical observations occurs during the 4th and 5th X-ray flares. We have estimated the X-ray continuum flux by extrapolating the X-ray flux observed at 1 ks to the time of the optical observation using a simple power law decay. We have then computed the broad band spectral index (α_{ox}) by connecting with a simple power law the *early* X-ray and optical fluxes. We obtain an X-ray to optical spectral index of $\alpha_{ox} = 0.98$. This value is not consistent with the X-ray spectral index ($\alpha = 0.74 \pm 0.07$). To match the α_{ox} value, we need the cooling frequency to be between the optical and X-ray bands. This hypothesis is impossible because the cooling frequency should still be above the X-ray band according to the closure relationships. We have also tried to use the mean X-ray flux during the flare, not correcting for the flare effect. Doing so, we obtain $\alpha_{ox} = 0.68$, now consistent with both X-ray and optical data taken separately. This may indicate that some flaring activity is also present in the optical light curve, not seen because of a poorly sampled optical light curve. In such a way, the initial steep optical decay is due to optical flares poorly sampled, while the late slow decay is the real continuum. This optical flaring activity, coincident with the late X-ray flares, may be expected : a clumpy medium can produce flares at optical and X-ray wavelengths in the afterglow if the cooling frequency is above the X-ray band.

The decay index (0.7 ± 0.2), and the spectral index (1.2 ± 0.3 , Tagliaferri et al. 2005b) of the *late* optical data are very different from the ones observed earlier. The closure relationships listed in Table 4 (last column) still discard a jet (as expected from the very low decay index). They would agree with a fast cooling mode, but this evolution (from slow cooling to fast cooling) is not physical. In the slow cooling mode, now both a wind and an ISM can fit the data assuming the cooling frequency to be below the optical band. However, assuming that the surrounding medium is still the wind medium, the expression of the cooling frequency is (Chevalier & Li 2000) :

$$\nu_c \sim 2 \times 10^{12} \left(\frac{1+z}{2} \right)^{-3/2} \left(\frac{\epsilon_B}{0.1} \right)^{-3/2} E_{52}^{1/2} A_*^{-2} t_d^{1/2} Hz \quad (1)$$

As one can see in Eqn. 1, the cooling frequency increases with time in the wind environment. Thus, the hypothesis that

the medium is still a wind and the cooling frequency has crossed the X-ray band is ruled out. This strengthen the possibility that the medium has changed from a wind to an ISM. Such a change is expected if there is a termination shock around the star (Ramirez-Ruiz et al. 2001; Chevalier et al. 2004), and we might observe for the first time the crossing of the termination shock by the fireball. Note that the time of this crossing is not well constrained. It occurs between 0.5 days (in the observer frame), and 0.02 days. If GRB 050904 was a typical burst at $z = 1 - 2$, this would have been observed before 0.2 days, which is the typical observation time of SWIFT (O'Brien et al. 2006). This crossing time is of the order of hte ones computed for 2 other bursts (GRB 990510 and GRB 000301C, Chevalier et al. 2004). The fact that such a crossing has never been reported yet may indicate that either the termination shock position of GRB 050904 is not typical or its effect in other bursts is very small. In the former hypothesis, the very large initial X-ray absorption (that imply a dense medium around that burst) may be the cause of a very nearby termination shock (see also Chevalier et al. 2004). Under this assumption the late X-ray flares have a natural explanation. The termination shock should not be an immediate discontinuity and should not be homogeneous (one may expect turbulences and clumps for a given time interval), thus producing density variations and consequently flares at all wavelength (see e.g. Dermer & Mitman 1999).

5. The first flare

With the Swift observations, it appears clear that flares are very common in GRB light curves during a time interval that goes from hundred to thousand of seconds (O'Brien et al. 2006). The evidence of such a common flaring activity has favored the development of several models that attempt to explain the nature of X-ray flares, both in the framework of Internal Shock and External Shock. In the following, we comment on the first X-ray flare in light of these models.

5.1. Delayed external shock scenario

The flare occurring in GRB 050904 is softer than the preceding plateau and is consistent with the following afterglow emission (see Sec. 3.1.2). Similar spectral properties have been previously observed in other bursts (e.g GRB 011121, XRR 011211 and XRF 011030, Piro et al. 2005; Galli & Piro 2005), and have been explained in the framework of a delayed external shock, expected e.g. in a thick shell fireball scenario (Sari & Piran 1999). In this framework both the X-ray and the optical flares are produced by the external shock, thus explaining the coincidence between the two flares.

Very recently, Lazzati et al. (2005) have shown that a central engine releasing most of its energy reservoir during the final stages of its activity (t_{eng}), implies that the afterglow emission is described by a simple power law only if the origin of the time t_0 is of the order of t_{eng} . We take this into account by adopting the method described in Galli & Piro (2005), thus assuming the beginning of the afterglow emission t_0 to be the time of flare appearance t_{flare} .

Table 4. Closure relationships in the standard fireball model computed using the spectral and temporal information. We express the relationships for the J band before and after 0.5 days. The specific frequency is defined as ν_c , the cooling frequency in the slow cooling mode, or ν_m , the injection frequency in the case of fast cooling. All errors are quoted at the 90 % confidence level.

Medium class and geometry	Cooling regime	Specific frequency position	Closure relationship	Expected value	X-ray (0.5-10.0 keV)	early optical (J band)	late optical (J band)
Isotropic Wind	Fast	$\nu_m < \nu$	$\delta - 1.5\alpha$	-0.5	0.6 ± 0.3	0.9 ± 0.9	-1.1 ± 0.6
		$\nu_m > \nu$	$\delta - 0.5\alpha$	0.0	1.2 ± 0.3	1.2 ± 0.4	0.1 ± 0.4
	Slow	$\nu_c < \nu$	$\delta - 1.5\alpha$	-0.5	0.6 ± 0.3	0.9 ± 0.9	-1.1 ± 0.6
		$\nu_c > \nu$	$\delta - 1.5\alpha$	0.5	0.6 ± 0.3	0.9 ± 0.9	-1.1 ± 0.6
Isotropic ISM	Fast	$\nu_m < \nu$	$\delta - 1.5\alpha$	-0.5	0.6 ± 0.3	0.9 ± 0.9	-1.1 ± 0.6
		$\nu_m > \nu$	$\delta - 0.5\alpha$	0.0	1.2 ± 0.3	1.2 ± 0.4	0.1 ± 0.4
	Slow	$\nu_c < \nu$	$\delta - 1.5\alpha$	-0.5	0.6 ± 0.3	0.9 ± 0.9	-1.1 ± 0.6
		$\nu_c > \nu$	$\delta - 1.5\alpha$	0.0	0.6 ± 0.3	0.9 ± 0.9	-1.1 ± 0.6
Jetted fireball	Slow	$\nu_c < \nu$	$\delta - 2\alpha$	0.0	0.6 ± 0.4	0.8 ± 1.3	-1.7 ± 0.8
		$\nu_c > \nu$	$\delta - 2\alpha$	1.0	0.6 ± 0.4	0.8 ± 1.3	-1.7 ± 0.8

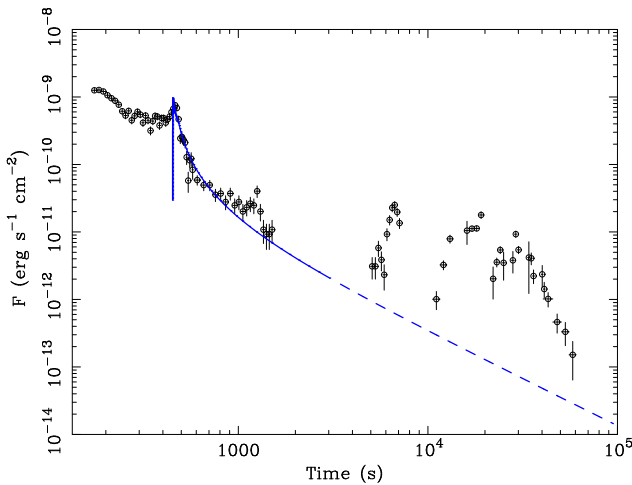


Fig. 5. X-ray light curve of GRB 050904 produced by a thick shell fireball expanding in a wind with the onset of the afterglow shifted to $t_0 = 464$ s. The model parameters are $E_{52}=100$, $\Gamma_0=400$, $A_*=0.01$, $\epsilon_e=0.01$, $\epsilon_B=0.0001$, $p=2.2$.

This model does not describe the termination shock transition, and thus cannot fit the *late* data. Consequently, we have applied it only to data before 2000 seconds. We used the temporal and spectral information derived in Sec. 3.1.2. The flare energy spectral index is $\alpha \sim 0.6$. The closure relationship values reported in Table 4 favor a fireball expanding in a wind with the cooling frequency ν_c above the X-ray band. According to the standard fireball model, in that case the spectral index is $\alpha = (p-1)/2$ (where p is the electron energy distribution power law index, Chevalier et al. 2004). We thus obtain $p = 2.2$. The isotropic energy released by the burst ranges from 6.6×10^{53} erg to 3.2×10^{54} erg as indicated by Cusumano et al. (2005). We have fixed it to $E_{52}=100$ (in the remaining we will use the standard notation $A_x = 10^x A$). The remaining model parameters, i.e. the wind parameter A_* , the fraction of energy going in relativistic electrons ϵ_e and the fraction of energy going in magnetic field ϵ_B are determined in order to describe the data.

We find a solution with parameters $\Gamma_0=400$, $A_*=0.01$, $\epsilon_e=0.01$, and $\epsilon_B=0.0001$, that can reproduce the observed X-

ray flare and the early X-ray afterglow (see Fig. 5), where Γ_0 represent the Lorentz Γ factor at the time of the flare. However this solution cannot reproduce the optical flare : the calculated optical flux at the time of the flare is $\sim 10^{-27}$ erg cm $^{-2}$ s $^{-1}$ Hz $^{-1}$, about 2.5 order of magnitude below the measured flux. In fact, if the cooling frequency ν_c is above the X-ray band, the predicted broad band optical to X-ray spectral index value (α_{ox}) should be 0.6. Instead, connecting the mean flux at 5 keV and the optical flux at the time of the flare, α_{ox} is ~ 1.1 . As a consequence the extrapolation of the X-ray flux in the I_T band falls below the optical data. A value of $\alpha_{ox} \sim 1.1$ at the time of the flare can be obtained assuming that ν_c is below the optical range during the flare, with $p = 2.2$, but this is not compatible with the closure relationships.

We thus conclude that there is not way to explain both the early X-ray and optical flares with only one emission component.

5.2. Other possible two-component scenarios

5.2.1. The role of the reverse shock

GRB 050904 is one of the five GRBs (the others are GRB 990123, GRB 041219A, GRB 050401, GRB 060111B) for which a prompt optical emission was observed simultaneously with the high energy one (Akerlof et al. 1999; Fan & Wei 2005; Rykoff et al. 2005; Boër et al. 2006; Klotz et al. 2006). Boër et al. (2006) underlined the similarities between GRB 990123 and GRB 050904 in terms of optical flare brightness (once accounting for the difference in the distance), and broadband spectrum of the prompt emission : in both cases the extrapolation of the high energy data to the optical band falls well below the optical points (Corsi et al. 2005; Boër et al. 2006), suggesting a different origin for the low and high energy emission mechanisms. In the case of GRB 990123, this hypothesis was further supported by the lack of coincidence between the peak observed in the optical and those observed in the high energy light curve (Corsi et al. 2005).

In the standard fireball model (Rees & Meszaros 1992; Meszaros & Rees 1997; Panaitescu et al. 1998), when a rel-

ativistic ejecta moves into the cold ISM, two shocks form, an outgoing one that propagates into the ISM (the Forward Shock, FS) and a Reverse Shock (RS) that propagates into the ejecta (Sari & Piran 1999).

The typical synchrotron frequency of the RS emission is in the IR-to-optical region. If the signal observed in the low-energy part of the prompt spectrum is related to the RS, while prompt γ - and X-ray emission to internal shocks (or late internal shocks for the late time X-ray flares), one should not expect the low energy emission to fall on the extrapolation of the high energy one; moreover, there should not be any correlation between the pulses observed in the high energy light curve and the peak time of the optical flare. This is in fact what was observed for GRB 990123. In the case of GRB 050904, the high energy spectrum cannot be extrapolated at low energies, but the optical flare observed by TAROT appears to peak simultaneously with the first X-ray flare. In the internal shock-RS scenario, such a coincidence should be fortuitous.

Recently Fan & Wei (2005) explored the possibility of relating X-ray flares to RS synchrotron emission appearing above the FS one, when the physical parameters (ϵ_e and ϵ_B) in the RS and the FS are different. In this framework, one could think of relating both the optical and the first X-ray flare to RS emission. The temporal coincidence between those two flares would be a natural expectation of this model. However, Wei et al. (2006) noted that even in this scenario, the X-ray spectrum should be a power-law extension of the optical emission, but the observations show that the optical-to-X-ray spectrum cannot be described by a simple synchrotron spectrum, even taking into account the possible presence of a spectral break between the optical and the X-ray band.

5.2.2. Flares in a RS synchrotron plus inverse Compton scenario

Recently, Kobayashi et al. (2005) suggested the possibility of explaining X-ray flares via synchrotron self-Inverse Compton (IC) radiation from the RS. The prompt optical flare should be associated with synchrotron emission from the RS while the simultaneous X-ray flare should be the result of synchrotron photons being up-scattered via the IC process in the X-rays. The RS evolution depends on the initial Lorentz factor of the shell itself (Sari 1997). In the so called thin shell case, the RS remains Newtonian during all the crossing time and the effective energy extraction takes place at the deceleration time t_d . On the other hand, if the initial Lorentz factor of the shell is sufficiently high, i.e. greater than the critical value Γ_c :

$$\Gamma_c \sim 130 \left(\frac{1+z}{2} \right)^{3/8} E_{52}^{1/8} T_2^{-3/8} n^{-1/8} \quad (2)$$

then the RS becomes relativistic while crossing the shell (Kobayashi et al. 2005). In Eq. 2, T is the burst duration. This correspond to the thick shell case. In a thin shell fireball expanding in an ISM, both the low and high energy emissions should thus peak at t_d and the temporal coincidence between the optical and the X-ray flares would be a natural expectation for this model too. In particular, in the thin shell case, the

peak time of the X-ray and optical flares (~ 460 s) constrains the model parameters according to the following relationship (Kobayashi et al. 2005):

$$t_d = 190 \left(\frac{\Gamma_0}{80} \right)^{-8/3} \left(\frac{1+z}{2} \right) E_{52}^{1/3} \left(\frac{n}{5} \right)^{-1/3} s \sim 460 s \quad (3)$$

Considering that $E_{52} \sim 10^2$ and that $z \sim 6.3$, for $n \sim 5$ it should be $\Gamma_0 \sim 165$, which gives $\Gamma_c \sim 230$ for $T \sim 225$ s, consistent with the hypothesis of being in a thin shell case (i.e. $\Gamma_0 < \Gamma_c$).

Using an additional emission mechanism like IC gives a natural explanation for the impossibility of extrapolating the spectrum of the X-ray flare down to the optical data points. In particular, we know that the 0.5–10 keV spectrum of the flare is rather flat, with a spectral index of $\alpha \sim 0.6$. Setting $p \sim 2.2$, the spectrum of the flare can be explained assuming that the X-ray band is between $\nu_m^{IC} = 2\gamma_m^2\nu_m$ and $\nu_c^{IC} = 2\gamma_c^2\nu_c$ around the deceleration time (Sari & Esin 2001). Considering that $\gamma_m \sim 100$, if $\nu_m^{IC} \sim 1.0$ keV and $\nu_c^{IC} \sim 10$ keV, then $\nu_m \sim 10^{13}$ Hz and $\nu_c \sim 3 \times 10^{13}$ Hz, that are reasonable values for the RS synchrotron break frequencies at the deceleration time (Kobayashi et al. 2005). With $p = 2.2$, the RS synchrotron flux at ~ 1 keV is $\sim 1/1500$ times the optical one. The ratio between the peak flux observed by TAROT between 449 s and 589 s, and the *mean flux* observed in the same temporal bin at 1 keV is $\sim 1/750$ (i.e. a factor of ~ 2 greater than that extrapolated from the RS synchrotron emission), while the ratio between the same optical flux and the *peak flux* of the X-ray flare at 1 keV is $\sim 1/280$ (i.e. a factor of ~ 5 greater than that extrapolated from the RS synchrotron emission). Thus, to explain the broad-band spectrum, the RS IC peak flux should be a factor of $\sim 2 - 5$ greater than the RS synchrotron flux at the same frequency (which is also compatible with the observed 2.0 – 6.0 keV flux increase by a factor of ~ 2 in the rising part of the flare). As shown by Kobayashi et al. (2005), an IC bump as high as 6 times the synchrotron RS emission can be explained with a reasonable choice of parameters.

The choice of the IC peak frequency being at about 1 keV at the deceleration time is not totally incidental: we have noted in section 3.1.2 that at the time of the flare, there is evidence for a transient rise in the value of the extragalactic absorption (see Table 1). This result was found assuming a simple power-law model for the spectrum. However, a spectral change below 1 keV could feature an increase in N_H : if the IC peak frequency is around 1 keV at the deceleration radius, we expect a spectral index of $\alpha = 1/3$ between 0.5 keV and 1 keV. To test this hypothesis, we fitted the data relative to the time bin in which the X-ray flare peaks, using a broken power-law model absorbed by our galaxy, with the N_H set to the Galactic value. The best fit values are: $\alpha_1 = 0.0_{-0.5}^{+0.3}$, $\alpha_2 = 0.6 \pm 0.2$, $E_{break} = 1.5 \pm 0.7$ keV, with a reduced χ^2 of 0.84 for 33 d.o.f. Adding a term of absorption locally to the GRB site, we find the extragalactic absorption to be consistent with 0 ($N_H < 5.0 \times 10^{22} \text{ cm}^{-2}$), thus solving the problem of the unexpected increase that was underlined in section 3.1.2. We stress that the fit with a broken power-law gives a spectral index of $\alpha_2 = 0.6 \pm 0.2$ above ~ 2 keV, which is the same as the one obtained with a single absorbed power-law;

moreover, the spectral index α_1 is consistent with the expected value of $1/3$, within the errors, and the fit is as good as the one obtained using a single power-law with additional absorption at the redshift of the burst ($\chi^2 = 0.96$ for 36 d.o.f.).

The model proposed by Kobayashi et al. (2005) thus appears to be a viable one to explain the broad-band spectrum and the temporal coincidence between the optical and the X-ray flares. However, one problem arises :

explaining the first X-ray flare via IC emission with $\nu_m^{IC} < \nu_X < \nu_c^{IC}$, implies that the decaying part of the flare should be as $(t/t_d)^{-(3p+1)/3}$ (Kobayashi et al. 2005), which for $p = 2.2$ gives $\delta = 2.5$, too shallow to agree with the observations (the X-ray emissions declines as $t^{-12.6}$ between 464 s and 534 s).

Moreover, in order for the RS emission to be dominant on the FS one, the peak frequency of the FS at the deceleration time should be $\nu_{syn}^{peak} \ll \nu_X$; combining this with the fact that the spectral index of the early X-ray afterglow is rather flat, it should be $\min(\nu_m, \nu_c) < \nu_X < \max(\nu_m, \nu_c)$ until $\sim 10^5$ s. However, as shown in Table 4, in this regime the expected temporal decay is too flat to be compatible with the observations.

Finally, the presence of a plateau before the optical flare observed by TAROT should also be considered: Wei et al. (2006) shown that a plateau plus an optical flare could be produced if the outflow had a more complex structure (e.g. two components with different Lorentz factors, widths and isotropic energies). However, a fit to the optical light curve gives a value for ϵ_B too high for being compatible with the idea of explaining the X-ray flare as IC emission from the RS. In fact, a high magnetization suppresses the importance of IC emission with respect to synchrotron one.

5.2.3. Internal shock scenario

Wei et al. (2006) have recently shown how the problem of the steep temporal decay of the X-ray flare can be solved invoking a late internal shock model, where the optical flash comes from late internal shock synchrotron emission while the first X-ray flare is produced by late internal shock IC emission. In this model the temporal coincidence between the optical and the X-ray flare is a natural expectation as it is in the model proposed by Kobayashi et al. (2005) and there is no optical to X-ray extrapolation problem.

Finally, Zou et al. (2005) interpreted the early-to-late time multi-band observations assuming that all the highly variable X-ray emission of GRB 050904 originated from internal shocks developing when faster shells, continuously ejected by the central engine, overtake a slower one. In this model, the main contribution to X-ray emission comes from relativistic RSs while the optical emission is ascribed to Newtonian FSs. Since this model is very different from the standard assumptions of the canonical fireball model, and seems to be able to fit the prolonged flaring activity observed in the X-rays, we will not discuss it further. However, we notice that the optical flare and the overall decay behavior of the X-ray light curve still need to be modeled in detail, even in this scenario. We also underline that this model assumes a super-long central engine

activity, i.e. that the shell ejection process lasts $10^4 - 10^5$ s, which has never been observed so far.

6. Conclusion

We have presented multi wavelength observations of GRB 050904 obtained with TAROT and SWIFT. We observed a flare simultaneously in the X-ray and optical light curves peaking at about 460 seconds after the burst. Before this flare, the X-ray decay and spectral indexes are consistent with the hypothesis of observing the tail of the prompt emission by curvature effect. After the flare, the X-ray emission is consistent with the hypothesis that the fireball expands in a wind medium. This would privilege a stellar progenitor. We note that it is the first time we can pinpoint a single star at that distance. Moreover, we observed before the flare a decrease of the X-ray column density that could be explained by photo-ionization of the medium by the burst. We investigated the simultaneity of the X-ray and optical flares in the context of several models. None of them can explain all the available data. At about 0.5 days, the optical light curve features a flattening that can be explained by the effect of the termination shock.

Due to the time dilation associated with its large distance GRB 050904 offered for the first time the possibility of well sampling the prompt to afterglow transition and the very early afterglow phase at several wavelengths. Its observation opened more questions than confirming canonical models. SWIFT is well suited to detect high redshift events, and hopefully other observations will be available to close those questions.

Acknowledgements. B.G. & G.S. acknowledge supports from the RTN "GRB : an enigma and a tool". We acknowledge financial supports from the French GDR PCHE. The TAROT telescope has been funded by the CNRS, the INSU, and the Carlsberg Foundation. It has been built with the support of the *division technique* of the INSU. We thank the technical staff contributing to the TAROT project : G. Bucholtz, J. Eysseric, C. Pollas, Y. Richaud.

References

- Akerlof, C., Balsano, R., Barthelmy, S. et al. 1999, *Nature*, 398, 400
- Arnaud, K.A., 1996, in ASP Conf. Ser. Vol. 101, *Astronomical Data Analysis Software and Systems V*, ed. G. Jacoby & J. Barnes, 17
- Barthelmy, S.D., Barbier, L.M., Cummings, J.R., et al., 2005, *Space Science Review*, in press, astro-ph/0507410
- Boër, M., Bringer, M., Klotz, A., et al. 1999, *A&AS*, 138, 579
- Boër, M., Atteia, J.L., Damerdjji, Y., et al., 2006, *ApJ*, 638, L71
- Burrows, D.N., Hill, J. E., Nousek, J. A., et al. 2005, *Space Science Review*, in press, astro-ph/0508071
- Burrows D. N., Romano, P.; Falcone, A., et al., 2005, *Science*, 309, 1833
- Burrows D. N., Romano, P.; Godet, O., et al., 2005, *X-Ray Universe 2005 conference proceedings*, astro-ph/0511039
- Chevalier, R.A., & Li, Z.Y., 1999, *ApJ*, 520, L29
- Chevalier, R.A., & Li, Z.Y., 2000, *ApJ*, 536, 195
- Chevalier, R.A., Li, Z.Y., & Fransson, C., 2004, *ApJ*, 666, 369
- Corsi, A., Piro, L., Kuulkers, E. et al. 2005, *A&A*, 438, 829

'GRB 050904' on page 7
'GRB 990123' on page 7
'GRB 990123' on page 8
'GRB 050904' on page 8
'GRB 050904' on page 9
'GRB 050904' on page 9
'GRB 050904' on page 9